A high-impact *COL6A3* mutation alters the response of chondrocytes in neo-cartilage organoids to hyper-physiologic mechanical loading

Niek GC Bloks[1,*], Zainab Harissa[2,3,*], Shaunak S Adkar[2,3], Amanda R Dicks[2,3], Ghazaleh Hajmousa[1], Nancy Steward[2,3] Roman I. Koning[1], Aat Mulder[1], Berend B.R. de Koning[1], Margreet Kloppenburg[1], Rodrigo Coutinho de Almeida[1], Yolande FM Ramos[1], Farshid Guilak[2,3,†], Ingrid Meulenbelt[1,†].

[1]Leiden University Medical Center, Leiden, The Netherlands,

[2]Washington University, Saint Louis, MO, USA

[3]Shriners Hospitals for Children, Saint Louis, MO, USA

[*]*Shared first author*

[†]*Shared last author*

What is already known:

- The etiology of osteoarthritis revolves around the interplay between genetic predisposition and perturbing environmental cues, such as mechanical stress.
- The pericellular matrix, with its hallmark proteins collagen type VI and fibronectin, surrounds the chondrocytes and is critical in transducing biomechanical cues from the extracellular matrix to chondrocytes henceforth it determines the chondrocyte mechanical environment.
- The mechanical environment of the chondrocytes is a critical factor that influences chondrocyte health as it determines the balance between synthesis and degradation of the articular cartilage extracellular matrix.

What this study adds:

- A sustainable human induced pluripotent stem cell-derived in-vitro neo-cartilage organoid model that is tailored to study detailed biologic effects of mechanical cues to chondrocytes.
- An OA disease-risk mutation in *COL6A3* reduces the binding between collagen type VI to fibronectin and provoked an osteoarthritic chondrocyte state.
- Upon hyper-physiological mechanical loading, aberrant function of the pericellular matrix, secondary to the *COL6A3* mutation, ablates the initial transient inflammatory response, characterized particularly by *PTGS2* encoding cyclooxygenase-2 (COX-2).

How this study might affect research practice or policy:

- Inhibiting COX-2, as an important transient inflammatory response after hyper-physiological mechanical cues, could worsen the loss of structural integrity of the cartilage in osteoarthritis patients. Henceforth, prescription of COX-2 inhibitors as pain treatment for OA patients should be reconsidered.

Abstract

Objectives: The etiology of osteoarthritis revolves around the interplay between genetic predisposition and perturbing environmental cues, such as mechanical stress. The pericellular matrix, with its hallmark proteins collagen type VI and fibronectin, surrounds chondrocytes and is critical in transducing the biomechanical cues. The objective is to study the functional effects of an OA disease-risk mutation in *COL6A3* in interaction with hyper-physiological mechanical cues in a tailored human induced pluripotent stem cells (hiPSCs) derived cartilage organoid model.

Method: To identify pathogenic OA mutations exome sequencing in symptomatic OA patients was performed. To study functional effects, CRISPR-Cas9 genome engineering was used to introduce the mutation in our established human induced pluripotent stem cell-derived in-vitro neo-cartilage organoid model in interaction with hyper-physiological mechanical loading conditions.

Results: A high-impact mutation in *COL6A3* was identified that resulted in significantly lower binding between the PCM proteins COLVI and fibronectin (FN) and provoked an osteoarthritic chondrocyte state. Moreover, aberrant function of the PCM, secondary to the *COL6A3* mutation, abolished the initial stress responses marked particularly by upregulation of *PTGS2* encoding cyclooxygenase-2 (COX-2), after hyper-physiological mechanical loading conditions.

Conclusion: These findings demonstrate that ablating the characteristic transient COX-2 response after injurious mechanical cues may have a direct negative impact on chondrocyte health.

Introduction

Osteoarthritis (OA) is a complex, multifactorial disease revolving around the interplay between genetic and environmental risk factors. In particular, biomechanical cues play a critical role in not only joint health but also drive the onset and progression of disease [1]. Indeed, physiologic levels of mechanical loading by virtue of physical exercise can slow down OA disease progression [2, 3]. In contrast, hyper-physiological loading, as seen with post-traumatic injuries such as articular fracture, meniscal tear, or rupture of the anterior cruciate ligament, concomitant with altered joint kinematics, is a major risk factor for the onset and progression of OA [4]. Both physiological and hyper-physiological loading results in alterations in the structural composition of the cartilage extracellular matrix [1]. These findings suggest that the balance of chondrocyte anabolic and catabolic processes for the maintenance of cartilage is tightly regulated by biomechanical cues.

Chondrocytes reside in a pericellular matrix (PCM), which modulates the transduction of mechanical cues from the extracellular matrix (ECM) towards the chondrocyte. The PCM for that matter contains specific proteins such as collagen 6 (COLVI) and fibronectin (FN) [5]. In particular, collagen 6 (COLVI) is involved in regulating the mechanical properties of the PCM as well as calcium signaling in response to mechanical stress [5-7]. Knock-out of a COLVI sub-unit, *COL6A1,* in a murine model induces an osteoarthritic phenotype through dysregulation of mechano-transduction [6, 8]. While loss of COLVI in humans is characterized by joint contractures, hyperlaxity, and myopathy resulting in an inability to ambulate [9], the effect of aberrant COLVI function on chondrogenesis and mechano-transduction remains unclear.

Here we report the identification of a *COL6A3* missense mutation through exome sequencing of affected sibling pairs with generalized OA. *COL6A3,* coding for one of the monomeric sub-units of COLVI [10] that resides in [6] and interacts with other PCM proteins [11, 12], is likely involved

78 in the regulation of cartilage structural composition and mechanical properties. We hypothesized
79 that the identified *COL6A3* mutation would perturb cartilage mechano-transduction in response to
80 hyper-physiologic loading, thereby contributing to OA pathogenesis. Recently, OA disease
81 modeling platforms utilizing human induced pluripotent stem cells (hiPSCs) have been used to
82 facilitate the interrogation of these pathogenic variants [13]. To gain an understanding of the role
83 of COLVI in cartilage, we studied this mutation in an *in vitro* model of OA using hiPSC-derived
84 cartilage. We employed genetically *COL6A3*-edited hiPSCs to an established *in vitro* cartilage
85 organoid model, and these neo-cartilage organoids were exposed to hyper-physiological
86 mechanical loading conditions. The effects of the mutation on COLVI's interaction with other
87 PCM proteins was studied. To study the downstream effects of this mutation in response to hyper-
88 physiologic mechanical loading conditions, we characterized downstream molecular pathways
89 based on transcriptome wide profiles. Understanding the role of COLVI in the regulation of
90 mechanical stress will provide insight into etiology of OA and guide the development of effective
91 treatment strategies for OA.

92

93 **Results**

94 *Identification of a damaging mutation in COL6A3*

95 Whole exome-sequencing was applied to a Caucasian sib pair of Dutch ancestry at age of 61
96 affected predominantly with symptomatic OA at multiple sites (GARP study) [14]. This resulted
97 in the detection of 81,416 genetic variants, after which a prioritization schema was followed to
98 identify pathogenic variants as previously described [15]. In short, first, we selected novel variants
99 in in-house whole genome sequencing projects (N=222) and the BBMRI-Genome of the

100 Netherlands project (GoNL, N=473) [15]. And second, damaging missense variants were selected
101 based on the prediction of sorting intolerant from tolerant (SIFT). This prioritization generated a
102 dataset of 38 novel coding variants that were predicted to have a functional impact on the protein
103 **(table S1)**. And third, these 38 novel coding variants were then further prioritized based on their
104 expression patterns in disease-relevant tissue by means of *in silico* analysis of 58 paired lesioned
105 and preserved samples, resulting in two genes that are highly expressed in cartilage and
106 differentially expressed between lesioned and preserved cartilage and bone; *MTHFR* (c.1667C>T,
107 p.Pro597Leu; cartilage: FC=0.84, FDR=0.04, bone: not detected) and *COL6A3* (c.4510C>T,
108 p.Arg1504Trp; cartilage: FC=1.75, FDR=2.25×10^{-5}, bone: FC=1.69, FDR=0.042) [16]. *MTHFR*
109 encodes for methylenetetrahydrofolate reductase, which is involved in folate metabolism [17].
110 *COL6A3* encodes for collagen VI subunit A3, which together with collagen VI subunit A1 and A2
111 forms a triple helical COLVI, a primary component of the cartilage PCM, and interacts with other
112 proteins such as fibronectin and hyaluronan [11, 12, 18]. The identified COL6A3 mutation is
113 located in the N-terminal VWA domains that are known to protrude away from the triple helical
114 structure. The *COL6A3* mutation was selected based on COLVI's role in regulating transduction
115 of mechanical cues in cartilage towards chondrocytes [6]. To gain an understanding of aberrant
116 COLVI function in cartilage, we selected this high-impact mutation for studying its effects in 3D
117 in-*vitro* models of cartilage, and in interaction with hyper-physiological mechanical loading
118 conditions.

119

120 *Introducing the mutation in hiPSCs*

121 To investigate the effects of the aberrant COLVI on COLVI-mediated matrix deposition and
122 molecular pathways, a gene-edited human induced pluripotent stem cell (hiPSC)-derived neo-
123 cartilage organoid model was generated. We employed CRISPR-Cas9 single-stranded
124 oligonucleotide-mediated homology-directed repair in hiPSCs to attain biallelic modification of
125 rs144223596 (c.4510C>T) in an isogenic background, which was confirmed by Sanger sequencing
126 **(Fig. S1)**. Although there was a small C peak visible at rs144223596, this was considered noise,
127 and as such we considered the clone to be homozygous. Next, the *COL6A3*-edited and the unedited
128 isogenic control hiPSCs were differentiated into chondrocytes using a previously established
129 chondrogenic differentiation protocol [19]. In short, hiPSCs followed a step-wise differentiation
130 protocol via mesodermal lineage differentiation towards chondroprogenitor cells [19]. These cells
131 were then dissociated, and chondrogenesis was initiated in our organoid pellet model.

132

133 *Characterization of the matrix of isogenic control and COL6A3 mutant hiPSC-derived cartilage*
134 *organoids*

135 Successful differentiation towards chondrocytes and the production of neo-cartilage was
136 confirmed by protein staining of collagen II (COLII), collagen VI (COLVI), and sulfated
137 glycosaminoglycans (sGAGs) **(Fig. 1A)**. COLII and COLVI deposition was not affected by the
138 mutation as measured by staining intensity **(Fig. 1B)**. However, quantification of sGAG
139 deposition, using the dimethyl methylene blue (DMMB) assay normalized to DNA content,
140 showed a significant reduction in the COLVI-mutant compared to the isogenic control neo-
141 cartilage organoids **(Fig. 1C)**. Next, the isogenic and COLVI-mutant neo-cartilage organoids were
142 characterized by targeted gene expression analysis using RT-qPCR of markers relevant for
143 cartilage homeostasis and mechano-transduction **(table 1).** The *COL6A3* mutation reduced

144 expression of the catabolic marker *ADAMTS5*, while also reducing expression of the anabolic
145 markers *COL2A1* as well as *ACAN*.
146

147 *Transmission electron microscopy of the cartilage neo-matrix*

148 To further investigate the effect of the mutation on the structural properties of the PCM and ECM,
149 we performed transmission electron microscopy. As shown in **Figure 2A,** there was a reduced
150 abundance of GAG-like structures in the *COL6A3*-mutant neo-cartilage organoids versus the
151 isogenic control. Consistent with the DMMB assay, upon performing quantitative analysis of these
152 GAG-like structures using a deep learning algorithm, we confirmed that mutant COLVI cartilage
153 had significantly decreased aggregate size (Fig.2B)and GAG abundance (Fig. 2C).
154

155 *Binding of isogenic control and COL6A3 mutant COLVI to pericellular matrix proteins*

156 The identified R1504W mutation is located in the N-terminal domain of COL6A3 coding for a
157 von Willebrand Factor A domain, which is involved in binding two important proteins in cartilage
158 PCM and ECM, fibronectin and hyaluronan [12, 13, 18]. Arginine at this position in the COL6A3
159 protein is evolutionary highly conserved, indicating that an amino acid change at this position is
160 likely to affect protein function **(Fig. S2)**. Thus, we hypothesized that the change from a polar
161 arginine to a non-polar tryptophan affects the interaction between COLVI and PCM/ECM proteins.
162 Hereto, we have performed a fibronectin and hyaluronan solid-phase binding assay with wild-type
163 and mutant COLVI, which was extracted from the chondrogenic differentiation medium of neo-
164 cartilage organoids. Results, as shown in Figure 2, demonstrated that binding to fibronectin was

reduced for mutant COLVI. However, we could not detect any binding of wild-type nor mutant COLVI to hyaluronan in our assay.

Effect of missense COL6A3 mutation on the transcriptomic landscape

Next, using RNA sequencing, we determined the downstream transcriptional effects of these changes in the PCM and ECM related to the *COL6A3* mutation. The stranded RNA sequencing allowed us to confirm the genotyping as performed with Sanger sequencing **(Fig S1)**, which revealed the inclusion of both heterozygous (n=9) and homozygous (n=17) samples in our dataset To avoid compromising on power in addition to detecting the most robust differentially expressed genes (DEGs), we have pooled these heterozygous and homozygous samples after correction. Multifactorial analysis revealed 3700 significant DEGs between the *COL6A3* mutant and isogenic controls (FDR<0.05) **(Fig. 4A, table S2)**. Among these genes, 55% were upregulated and 45% were downregulated. Notable highly significant DEGs were related to development and cartilage metabolism, with the downregulation of structural PCM and ECM proteins, such as *COL27A1* and *PRG4*, increased catabolic activity, such as *MMP9*, and ECM mineralization, such as *SPP1* **(Fig. 4A-B)**.

To determine the biological processes associated with the *COL6A3* mutation, we performed a weighted gene co-expression network analysis (WGCNA) [20] on the RNA-sequencing data set. This resulted in the detection of 20 distinct co-expression networks **(Fig. S3)**. Multifactorial regression analysis revealed 10 co-expression networks with the first principal component significantly associated with the *COL6A3* genotype **(Fig. S3)**. The top 3 most significant co-expression networks associated with the *COL6A3*-mutant genotype were enriched for

187 developmental processes, cell-cell adhesion/anatomical structure morphogenesis, and ECM
188 organization **(Fig. 4C)**. Enrichment of ECM organization again underlines the detrimental effects
189 of the *COL6A3* mutation on the development of cartilage, affecting genes such as *LAMA5*, *LAMB2,*
190 and *COL18A1* that code for structural PCM components **(Fig. 4D)**. While enrichment of cell-cell
191 adhesion pathways suggests that the mutation also affects mechano-transduction via altered cell-
192 cell adhesion by downregulation of cadherin-associated genes**,** such as *CDH18*, *CDH6*, *PTGER4*,
193 *MAPK14,* and *ADAMTS5* **(Fig. S4)**. Of note is that *ADAMTS5* is downregulated in the *COL6A3*
194 mutant while quantification of sGAGs, the target peptides of ADAMTS5 cleavage, are reduced at
195 both the gene level (*ACAN*, **Table 1**) and protein level **(Fig. 1C; Fig. 3A-C).**
196 To study the relevance of the *COL6A3* mutation to OA pathophysiology, we determined the
197 overlap of gene expression between the effects of the *COL6A3* mutation and the differential
198 expression between lesioned and preserved cartilage from patient material collected post-joint
199 replacement surgery in a previously published dataset containing 58 paired samples [16] revealing
200 a subset of 582 overlapping DEGs **(table S4)**. We then performed pathway analysis on this subset
201 of genes **(Fig. 4B)**. The most significant enriched pathway was skeletal system development,
202 including transcription factors (*RUNX3*, *TNFRSF11B*), ECM components (such as *COL27A1*,
203 *COL11A2*), and anabolic factors (such as *IGF1*, *BMP3*). Well-known pathways related to
204 inflammation "inflammatory response" and "acute inflammatory response" were also enriched
205 containing inflammatory cytokines (IL31a) and general inflammatory response factors (*PTGES*,
206 *HLA-e*). Also, the "ossification" pathway was enriched, containing OA risk genes (*SPP1*, *TNC,*
207 and *MGP*). Genes related to cartilage metabolism were confirmed by quantitative reverse
208 transcription polymerase chain reaction (RT-qPCR) **(table S5).** Together, this data suggests that

209 the *COL6A3* mutation results in downstream expression changes, in part describing the
210 osteoarthritis pathophysiology.
211 Additionally, to explore the effect of the hetero- and homozygous *COL6A3*-mutated hiPSC-
212 derived neo-cartilage organoids, a dose-response effect was modeled for DEGs (FDR<0.05)
213 responding to the *COL6A3* mutation. To this end, the hetero- and homozygous *COL6A3* mutation
214 was considered as a covariate and analyzed for differential expression. This revealed a robust dose-
215 response effect (FDR<0.05) of the *COL6A3* mutation on gene expression in 2610 genes out of the
216 3700 DEGs affected by the mutation, **(table S6; Figure S6**), such as MMP9, PRG4, and SPP1
217 This dose-response effect further underlines the biological validity of the gene expression changes
218 due to *COL6A3* mutation.
219 Taken together, we showed that the *COL6A3* mutation reduces sGAG deposition **(Fig. 1)**, reduces
220 binding to fibronectin **(Fig. 2)**, and lowers the expression of mechano-sensor genes **(table 1)**
221 suggesting the mutation could affect the transduction of mechanical cues. Hence, we determined
222 whether the *COL6A3* mutation affects the transcriptomic response to hyper-physiologic
223 mechanical loading conditions. Hereto, two different organoid models were applied; cylindrical
224 constructs in which hiPSC-derived pellets were digested to obtain single-cell chondrocytes that
225 were then encapsulated in an agarose gel, and spherical constructs with neo-cartilage deposited by
226 hiPSC-derived chondrocytes. Both these organoid models were exposed to hyper-physiologic
227 mechanical loading conditions [20% sinusoidal peak-to-peak strain at 5hz for 10 minutes].
228 Transcriptional activity was measured 12 hours after mechanical stimulation in isogenic controls
229 (unloaded isogenic controls - n=13, mechanically stimulated isogenic controls - n=13) as well as
230 *COL6A3*-mutant (unloaded *COL6A3* mutants – n=14 and mechanically loaded *COL6A3* mutants -
231 n=12) organoids.

232

233 *Effect of mechanical loading on the transcriptomic landscape*

234 Next, we characterized the effect of hyper-physiologic loading conditions [21] on these neo-
235 cartilage organoids. Multifactorial analyses revealed 177 DEGs (FDR<0.05) between unloaded
236 and mechanically loaded organoids, of which 74% were upregulated and 26% were downregulated
237 **(Fig.6A, table S7)**. Notable genes were, amongst others; *CD44*, *CAV1*, *ITGA5* **Fig. 6B**), which are
238 all genes encoding for mechano-sensors involved in OA pathophysiology.
239 To determine the biological processes affected by hyper-physiologic mechanical loading WGCNA
240 co-expression networks were associated with mechanical loading, revealing 5 significantly
241 associated co-expression networks **(Fig. S2; table S3)**. The top 3 most significantly associated
242 modules were enriched for developmental and signaling processes, stress responses**,** and neuronal
243 pathways **(Fig. 6B)**. While enrichment of signaling responses containing genes such as *IL1RL1*
244 and *FOSL1* show an adaptive response to hyper-physiologic mechanical loading conditions **(Fig.**
245 **6D)**, enrichment of stress responses with genes such as *HSPA1B* and *DNAJA4* underlines the
246 damaging effects of the hyper-physiologic mechanical loading conditions **(Fig 6E).**

247

248 *Effect of the COL6A3 missense mutation on the response to hyper-physiological mechanical*
249 *loading conditions*

250 Finally, the effects of the *COL6A3* mutation on the response to hyper-physiological mechanical
251 loading were investigated. To this end, a multifactorial analysis was performed resulting in a set
252 of 135 genes with a significant interaction effect (P<0.01) indicating that the mutation affected the
253 response to hyper-physiological mechanical loading **(table S8)**. Of these 135 genes, 70 proteins

254 show a significant protein-protein interaction (PPI) (FDR<0.05) as determined by STRING-DB
255 **(Fig. 7A)**. Notable is that highly connected genes in this PPI network such as; *PTGS2*, *IL1R1,*
256 *IRAK2, PECAM1,* and *ADAMTS5* are all related to catabolic and inflammatory signaling. *PTGS2*
257 is known to be regulated by TRPV4 signaling in response to mechanical stress [22] and is involved
258 in inducing an inflammatory response to stimuli [23]. *IL1R1* codes for the receptor of interleukin-
259 1, one of the key inflammatory markers in OA, and thus is involved in inflammatory signaling,
260 while *IRAK2* encodes for the interleukin-1 receptor-associated kinase 2, which is involved in
261 interleukin-1 (IL-1) induced upregulation of NF-κβ [24]. Upon performing stratified analysis, it
262 was shown that the interaction effect was particularly caused by an upregulation of gene expression
263 observed in isogenic controls in response to hyper-physiological loading conditions, that appeared
264 absent in the *COL6A3* mutant neo-cartilage organoids **(Figure 7B; table S9).**
265 To study the biological processes in which the response to hyper-physiological loading differed
266 between the isogenic control and the *COL6A3* mutants, associate this interaction effect with the
267 principal component of each detected co-expression network. This revealed three distinct co-
268 expression networks associated with the interaction effect, which were enriched for processes
269 related to signaling, ECM organization, and general biological processes **(Figure 7C)**. Enrichment
270 of pathways related to signaling shows an aberrant response in genes such as *INHBA* which acts
271 downstream of TRPV4 calcium channels [22], *CAV1*, *SEMA7A*, and *MMP3,* which are all genes
272 that respond to mechanical loading in isogenic controls, with an absent loading effect in the
273 *COL6A3* mutant **(table S3)**. Again, the enrichment of processes related to ECM formation and
274 organization, containing genes such as; *MMP13, RUNX1, FN1, LAMC1, EGFR,* and *PMEPA1*
275 **(Fig. 7D)**, underlines the effect of an impaired repair response to hyper-physiological mechanical
276 loading conditions in the *COL6A3* mutant. Also, the enrichment of general biological processes

277 including *IL1R1* highlights the aberrant response to mechanical loading in the *COL6A3* mutant
278 neo-cartilage organoids.

279

280 **Discussion**

281 In the current study, we identified a missense mutation in *COL6A3* (c.4510C>T, p.Arg1504Trp)
282 in a sibling pair of the GARP-study affected with symptomatic OA in two or more joint sites [14].
283 By introducing this high-impact mutation in hiPSCs using CRISPR-Cas9 genome engineering
284 while employing these cells in an established 3D *in vitro* neo-cartilage organoid model, we showed
285 that the mutation decreases cartilage matrix integrity, as reflected by a reduction in abundance and
286 size of GAGs. Moreover, by subsequently isolating mutated COL6 protein, we showed that the
287 mutation reduced binding to fibronectin. Analysis of the transcriptome-wide gene expression
288 changes with *COL6A3* mutation showed overlap with transcriptomic changes due to OA-
289 pathophysiology [16] indicating that an osteoarthritic chondrocyte state appeared secondary to
290 alterations in PCM function due to mutant *COL6A3.* Finally, by exposing the neo-cartilage
291 organoids to hyper-physiological mechanical stress, we demonstrated that mutated *COL6A3*
292 abolished the characteristic upregulation of inflammatory signaling after mechanical loading [21,
293 22, 25] with *PTGS2*, *PECAM1*, and *ADAMTS5*, as most central and notable genes. Taken together,
294 our findings suggest that the identified mutation in COL6A3 resulted in impaired binding between
295 COLVI and the PCM protein fibronectin and abolished the initial stress response to hyper-
296 physiologic mechanical loading conditions that could affect the propensity of the chondrocyte to
297 enter an OA disease state.

298 Although it has been suggested that *PTGS2*, commonly known as cyclooxygenase-2 (COX-2), as
299 part of the PGE2–EP4 axis, is essential to initiate repair in other tissues in response to stressors
300 [26], we here showed for the first time that absence of this COX-2 response could underlie OA
301 pathophysiology. Notable in this respect is that COX-2 inhibitors are frequently prescribed for OA
302 pain [27]. In light of our result, we advocate that increased joint loading upon prescription of COX-
303 2 inhibitors for OA pain could worsen OA pathophysiology.
304 By introducing an high-impact *COL6A3* mutation in a hiPSC-derived neo-cartilage organoid
305 model that had been genome-edited via CRISPR-Cas9 to harbor this mutation, we have been able
306 to study in detail chondrocyte mechano-biologic effects to hyper-physiological mechanical stress.
307 Nonetheless it should be noted that upon checking the homozygous introduction of the *COL6A3*
308 mutation by genotyping the RNA sequencing data, heterozygous *COL6A3* mutated samples were
309 identified. These heterozygous *COL6A3* mutant cells could have arisen due to a selective
310 advantage upon expanding hiPSCs. Availability of hetero- and homozygous samples, however,
311 did allow us to study a possible dose-response effect of the mutation on RNAseq data and
312 confirmed a dose-response effect in 2610 genes out of the 3700 DEGs. This adds to the validity of
313 our data and biological relevance of the studied *COL6A3* mutation, as there was an additive effect
314 of the hetero- and homozygous *COL6A3* mutants on DEGs such as SPP1, MMP9, and PGR4 **(table**
315 **S6, Fig. S7)**.
316 We have applied both cylindrical disc-shaped organoids [22] as well as spherical pellets [13, 21].
317 The advantage of the first model is an ensured equal distribution of mechanical stress throughout
318 the disc-shaped sample. The advantage of the second model is that it allows harnessing the original
319 matrix deposited by the hiPSC-derived chondrocytes thereby permitting the characterization of
320 changes in the ECM. Additionally, this model of hyper-physiological loading in hiPSC neo-

321 cartilage organoids can be expanded to define and apply more beneficial mechanical loading
322 regimes, further unraveling the shift in molecular mechanisms underlying the normal physiological
323 response to loading that might further aid in the development of treatment strategies.
324 In contrast to previous findings [12], we could not detect any binding of COLVI with hyaluronan,
325 which might be explained by the source of the COLVI proteins, as they were extracted from the
326 culture medium. Alternatively, other intermediary proteins are necessary for binding COLVI to
327 hyaluronan which might not have been present in the medium [11]. Moreover, we have used TEM
328 in combination with a, yet to be published, machine-learning tool to detect changes in GAG size
329 and abundance. We relied on the similarity with previously published data to train the machine-
330 learning algorithm. Nevertheless, the reduced abundance of GAGs as measured with TEM is in
331 line with the results of the DMMB assay, as well as the Alcian blue staining.
332 By using genetic engineering of hiPSC-derived neo-cartilage organoids while implementing
333 hyper-physiological mechanical loading conditions, we established a tailored model to study the
334 biological function of proteins in the transduction of mechanical cues from ECM to chondrocytes.
335 By using this model, we here showed that an identified OA disease-risk mutation in COL6A3
336 reduces the binding between collagen type VI to fibronectin and provoked an osteoarthritic
337 chondrocyte state. Moreover, we are among the first to demonstrate that aberrant function of
338 COLVI in the PCM abolishes the initial inflammatory response to hyper-physiological loading, as
339 marked by, amongst others, changes in *PTGS2* encoding COX-2. In light of these finding, we
340 advocate that COX-2 inhibitors prescribed as pain medication to OA patients could have a
341 negative impact on chondrocyte health when patients are exposed to hyper-physiological
342 mechanical loading.

343

344 **Materials and Methods**

345

346 *Exome sequencing*

347 Exome sequencing of a sibling pair with generalized OA at multiple joint sites was performed by
348 Illumina HiSeq 2000 technology (Beijing Genome Institute) using the protocol described in the
349 supplementary methods.

350

351 *hiPSC line and cell culture*

352 An hiPSC line as described earlier was used as the unedited isogenic control [19]. In short, RVR-
353 iPSC line was retrovirally reprogrammed from BJ fibroblasts and characterized. Further culture
354 conditions can be found in the supplementary methods.

355

356 *Genome editing of hiPSCs*

357 We employed CRISPR-Cas9 single-stranded oligonucleotide-mediated homology-directed repair
358 in hiPSCs to attain biallelic modification of rs144223596 (c.4510C>T) in an isogenic background,
359 Additional information on the genomic target, guide sequences and transfection protocol can be
360 found in the supplementary methods.

361

362 *hiPSC differentiation to induced chondrocytes*

363 Generation of induced chondroprogenitor cells (hiCPCs) was based on a protocol previously
364 described [19] which was shown to produce similar neo-cartilage to that produced by human
365 primary articular chondrocytes [28] further described in the supplementary methods.

366

367 *Mechanical loading*

368 The spherical-shaped neo-cartilage constructs were mechanically loaded using a MACH-1
369 mechanical testing device (Biomomentum), at a rate of 5hz with 20% sinusoidal peak-to-peak
370 strain for 10 minutes as described earlier [21]

371

372 *sGAG measurement*

373 Sulfated glycosaminoglycan (sGAG) concentrations in the neo-cartilage organoids (µg sGAG/µg
374 DNA) were measured using the Farndale Dimethyl Methylene Blue (DMMB, Sigma) method [29].
375 Additional information can be found in the supplementary methods.

376

377 *Histology and immunohistochemistry*

378 Neo-cartilage samples were fixed in 4% formaldehyde and embedded in paraffin. Sections were
379 stained with Alcian Blue (Sigma-Aldrich) and Nuclear Fast Red (Sigma-Aldrich). Deposition of
380 collagen II and collagen VI in the neo-cartilage constructs was visualized immunohistochemically
381 according to the protocol described in the supplementary methods.

382

383 *RT-qPCR*

384 Per sample, two replicate mRNA samples were measured in triplicates in a MicroAmp™ Optical
385 384-Well Reaction Plate (ThermoFisher Scientific), using the QuantStudio™ Flex Real-Time PCR
386 system (Applied Biosystems™). Additional information can be found in the supplementary
387 methods.

388

389 *RNAseq*

390 RNA from neo-cartilage constructs was extracted 12 hours post mechanical loading and analyzed
391 using the Illumina NOVAseq 6000. Additional information on RNA isolation, mapping,
392 alignment, and data processing and analysis can be found in the supplementary methods.

393

394 *Solid-phase binding assay*

395 Conditioned medium of wild-type and *COL6A3* mutant organoids was collected and concentrated
396 in preparation for the binding assay. To this end, 450 µl of medium was collected in 100 K
397 molecular weight cutoff Pierce Protein Concentrators (Thermo Scientific) and centrifuged for 10
398 min at 12,000g. Subsequently, COL6 concentration was determined using the Human COL6A3
399 ELISA Kit (Assay Genie) according to the manufacturer's protocol which can be found in the
400 supplementary methods.

401

402 *Transmission electron microscopy*

403 To the neo-cartilage organoids, consisting of cells and matrix, a previously established protocol
404 was used to perform TEM. Additional information on sample processing, image acquisition,
405 processing and analysis can be found in the supplementary methods.

406

407 *Statistical analysis*

408 For all data analysis except RNA sequencing we have used a generalized linear model including
409 the factors hyper-physiological loading and the *COL6A3* mutation using R statistical software
410 version 4.1.1.

411

412 **References**

413 1. Guilak, F., *Biomechanical factors in osteoarthritis.* Best Pract Res Clin Rheumatol, 2011.
414 **25**(6): p. 815-23.
415 2. Juhl, C., et al., *Impact of exercise type and dose on pain and disability in knee*
416 *osteoarthritis: a systematic review and meta-regression analysis of randomized*
417 *controlled trials.* Arthritis Rheumatol, 2014. **66**(3): p. 622-36.
418 3. Uthman, O.A., et al., *Exercise for lower limb osteoarthritis: systematic review*
419 *incorporating trial sequential analysis and network meta-analysis.* BMJ, 2013. **347**: p.
420 f5555.
421 4. Olson, S.A. and F.J.P. Guilak, *Post-traumatic Arthritis.* 2015.
422 5. Guilak, F., et al., *Osteoarthritis as a disease of the cartilage pericellular matrix.* Matrix
423 Biol, 2018. **71-72**: p. 40-50.
424 6. Zelenski, N.A., et al., *Type VI Collagen Regulates Pericellular Matrix Properties,*
425 *Chondrocyte Swelling, and Mechanotransduction in Mouse Articular Cartilage.* Arthritis
426 Rheumatol, 2015. **67**(5): p. 1286-94.
427 7. Guilak, F., et al., *The pericellular matrix as a transducer of biomechanical and*
428 *biochemical signals in articular cartilage.* Ann N Y Acad Sci, 2006. **1068**: p. 498-512.
429 8. Alexopoulos, L.G., et al., *Developmental and osteoarthritic changes in Col6a1-knockout*
430 *mice: biomechanics of type VI collagen in the cartilage pericellular matrix.* Arthritis
431 Rheum, 2009. **60**(3): p. 771-9.
432 9. Bonnemann, C.G., *The collagen VI-related myopathies: muscle meets its matrix.* Nat Rev
433 Neurol, 2011. **7**(7): p. 379-90.
434 10. Beecher, N., et al., *Collagen VI, conformation of A-domain arrays and microfibril*
435 *architecture.* J Biol Chem, 2011. **286**(46): p. 40266-75.

436 11. Wiberg, C., et al., *Complexes of matrilin-1 and biglycan or decorin connect collagen VI*
437 *microfibrils to both collagen II and aggrecan.* J Biol Chem, 2003. **278**(39): p. 37698-704.
438 12. Specks, U., et al., *Structure of recombinant N-terminal globule of type VI collagen alpha*
439 *3 chain and its binding to heparin and hyaluronan.* 1992. **11**(12): p. 4281-4290.
440 13. van Hoolwerff, M., et al., *High-impact FN1 mutation decreases chondrogenic potential*
441 *and affects cartilage deposition via decreased binding to collagen type II.* Sci Adv, 2021.
442 **7**(45): p. eabg8583.
443 14. Riyazi, N., et al., *Risk factors in familial osteoarthritis: the GARP sibling study.*
444 Osteoarthritis Cartilage, 2008. **16**(6): p. 654-9.
445 15. Kiezun, A., et al., *Deleterious alleles in the human genome are on average younger than*
446 *neutral alleles of the same frequency.* PLoS Genet, 2013. **9**(2): p. e1003301.
447 16. Coutinho de Almeida, R., et al., *RNA sequencing data integration reveals an miRNA*
448 *interactome of osteoarthritis cartilage.* Ann Rheum Dis, 2019. **78**(2): p. 270-277.
449 17. Welch, G.N. and J.J.N.E.j.o.m. Loscalzo, *Homocysteine and atherothrombosis.* 1998.
450 **338**(15): p. 1042-1050.
451 18. Keesler, D.A., et al., *Fibronectin binding to von Willebrand factor occurs via the A1*
452 *domain.* Res Pract Thromb Haemost, 2021. **5**(5): p. e12534.
453 19. Adkar, S.S., et al., *Step-Wise Chondrogenesis of Human Induced Pluripotent Stem Cells*
454 *and Purification Via a Reporter Allele Generated by CRISPR-Cas9 Genome Editing.*
455 Stem Cells, 2019. **37**(1): p. 65-76.
456 20. Zhang, B., S.J.S.a.i.g. Horvath, and m. biology, *A general framework for weighted gene*
457 *co-expression network analysis.* 2005. **4**(1).
458 21. Timmermans, R.G.M., et al., *A human in vitro 3D neo-cartilage model to explore the*
459 *response of OA risk genes to hyper-physiological mechanical stress.* Osteoarthritis and
460 Cartilage Open, 2022. **4**(1).
461 22. Nims, R.J., et al., *A synthetic mechanogenetic gene circuit for autonomous drug delivery*
462 *in engineered tissues.* 2021. **7**(5): p. eabd9858.
463 23. Simon, L.S., *Role and regulation of cyclooxygenase-2 during inflammation.* The
464 American journal of medicine, 1999. **106**(5): p. 37S-42S.
465 24. Guo, F., Y. Li, and S.J.I. Wu, *Antisense IRAK-2 Oligonucleotide Blocks Il-1-Stimulated*
466 *NF-κB Activation and ICAM-1 Expression in Cultured Endothelial Cells.* 1999. **23**(6): p.
467 535-543.
468 25. Vincent, T.L., *Mechanoflammation in osteoarthritis pathogenesis.* Semin Arthritis
469 Rheum, 2019. **49**(3S): p. S36-S38.
470 26. Miyoshi, H., et al., *Prostaglandin E2 promotes intestinal repair through an adaptive*
471 *cellular response of the epithelium.* EMBO J, 2017. **36**(1): p. 5-24.
472 27. Puljak, L., et al., *Celecoxib for osteoarthritis.* Cochrane Database Syst Rev, 2017. **5**: p.
473 CD009865.
474 28. Rodriguez Ruiz, A., et al., *Cartilage from human-induced pluripotent stem cells:*
475 *comparison with neo-cartilage from chondrocytes and bone marrow mesenchymal*
476 *stromal cells.* Cell Tissue Res, 2021. **386**(2): p. 309-320.
477 29. Farndale, R.W., C.A. Sayers, and A.J. Barrett, *A Direct Spectrophotometric Microassay*
478 *for Sulfated Glycosaminoglycans in Cartilage Cultures.* Connective Tissue Research,
479 1982. **9**(4): p. 247-248.
480 30. Kent, W.J., et al., *The human genome browser at UCSC.* 2002. **12**(6): p. 996-1006.

481 31. Wu, T.D. and C.K. Watanabe, *GMAP: a genomic mapping and alignment program for*
482 *mRNA and EST sequences.* Bioinformatics, 2005. **21**(9): p. 1859-75.
483 32. Anders, S., P.T. Pyl, and W. Huber, *HTSeq--a Python framework to work with high-*
484 *throughput sequencing data.* Bioinformatics, 2015. **31**(2): p. 166-9.
485 33. Ewels, P., et al., *MultiQC: summarize analysis results for multiple tools and samples in a*
486 *single report.* Bioinformatics, 2016. **32**(19): p. 3047-8.
487 34. Leek, J.T., *svaseq: removing batch effects and other unwanted noise from sequencing*
488 *data.* Nucleic Acids Res, 2014. **42**(21).
489 35. Love, M.I., W. Huber, and S. Anders, *Moderated estimation of fold change and*
490 *dispersion for RNA-seq data with DESeq2.* Genome Biol, 2014. **15**(12): p. 550.
491 36. *<Benjamini, Hochberg, Society - 2018 - Controlling the False Discovery Rate A*
492 *Practical and Powerful Approach to Multiple Testing Author.pdf>.*
493 37. Langfelder, P. and S.J.B.b. Horvath, *WGCNA: an R package for weighted correlation*
494 *network analysis.* 2008. **9**(1): p. 1-13.
495 38. Szklarczyk, D., et al., *STRING v11: protein–protein association networks with increased*
496 *coverage, supporting functional discovery in genome-wide experimental datasets.* 2019.
497 **47**(D1): p. D607-D613.
498 39. Reynolds, E.J.J.C.B., *Thc use ol lead Citrate at high pH as an electron-opaque stain in*
499 *electron microscopy.* 1963. **17**: p. 20&-212.
500 40. Faas, F.G., et al., *Virtual nanoscopy: generation of ultra-large high resolution electron*
501 *microscopy maps.* J Cell Biol, 2012. **198**(3): p. 457-69.

502

503 **Acknowledgments**

504 **Funding:** Leiden University Medical Centre, Pfizer Groton, Connecticut, USA and the Dutch
505 Arthritis Society have supported the GARP study. Furthermore, the research leading to these
506 results has received funding from the Biobanking and BioMolecular resources Research
507 Infrastructure the Netherlands (BBMRI-NL) (complementation project CP2013-84), the Dutch
508 Scientific Research council NWO/ZonMW VICI scheme (nr. 91816631/528) and the Dutch
509 Arthritis Society. We are indebted to drs. N. Riyazi, J. Bijsterbosch, H.M. Kroon and I. Watt for
510 collection of data. Furthermore, this work was supported by the Shriners Hospitals for Children
511 and the NIH (grants AG46927, AG15768, AR080902, AR072999, AR073752, and AR074992).
512 Additionally, the data is generated within the scope of the Medical Delta programs Regenerative

513 Medicine 4D: Generating complex tissues with stem cells and printing technology and Improving
514 Mobility with Technology.
515
516 **Author Contributions:** N.G.C.B., Z.H., A.R.D., Y.F.M.H, F.G., I.M. developed the concept of
517 this study; N.G.C.B., Z.H., S.S.A., A.R.D., G.H., N.S. M.K., R.I.K., A.A.M., B.B.R.K. and F.G.,
518 acquired materials and data; N.G.C.B., R.C.D.A., B.B.R.K., Y.F.M.H, F.G. and I.M. analyzed the
519 data; and all authors contributed to the writing of the manuscript.

520 **Competing interests:** F.G. is an employee and shareholder in Cytex Therapeutics Inc. The authors
521 declare that they have no other competing interests.

522 **Data and materials availability:** All data needed to evaluate the conclusions in the paper are
523 present in the paper and/or the Supplementary Materials.

524

525 **Figures and Tables**

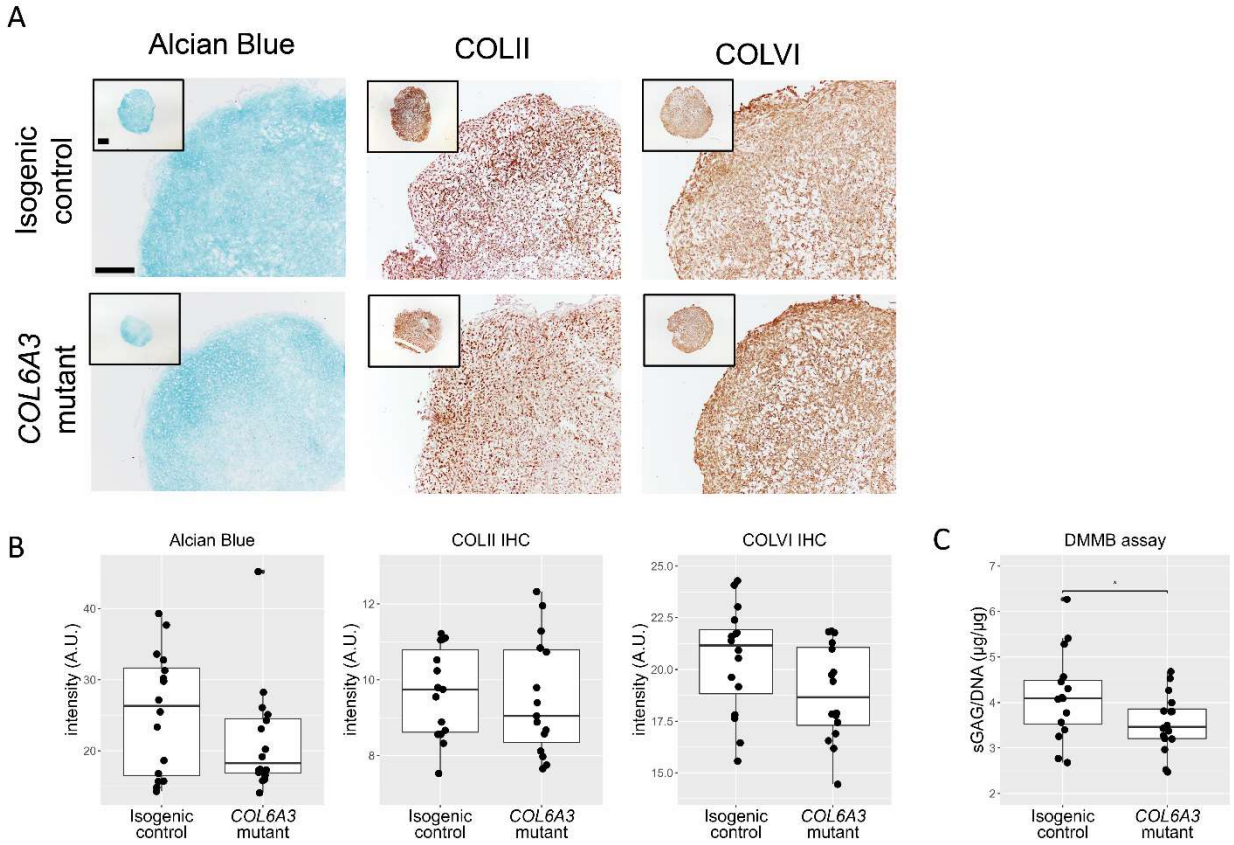

526

527 **Figure 1. Effect of the mutation on neo-cartilage matrix deposition. (A)** Representative images
528 of Alcian blue staining marking sulfated glycosaminoglycans (sGAGs) and immunohistological
529 staining of collagen II (COL II) and collagen VI (COLVI). Scale bar 200µm. **(B)** Quantification
530 of Alcian blue, COLII, and COLVI in isogenic control and *COL6A3*-mutant neo-cartilage
531 organoids showed no significant effect of the mutation (N=16). **(C)** Quantification of sGAG
532 deposition in neo-cartilage organoids. sGAG deposition in COLVI-mutant neo-cartilage organoids
533 is reduced in comparison to isogenic controls (beta=0.55 ± 0.28, P=4.9x10^{-2}, N=16). Statistics are
534 reported as beta ± standard error. The box plots represent 25th, 50th, and 75th percentiles, and
535 whiskers extend to 1.5 times the interquartile range. Individual samples are depicted by black dots

536 in each graph. P values were attained using a generalized linear model with intensity (for immuno-
537 stainings) and (sGAGs/DNA) as dependent variable and genotype as independent variable.

538

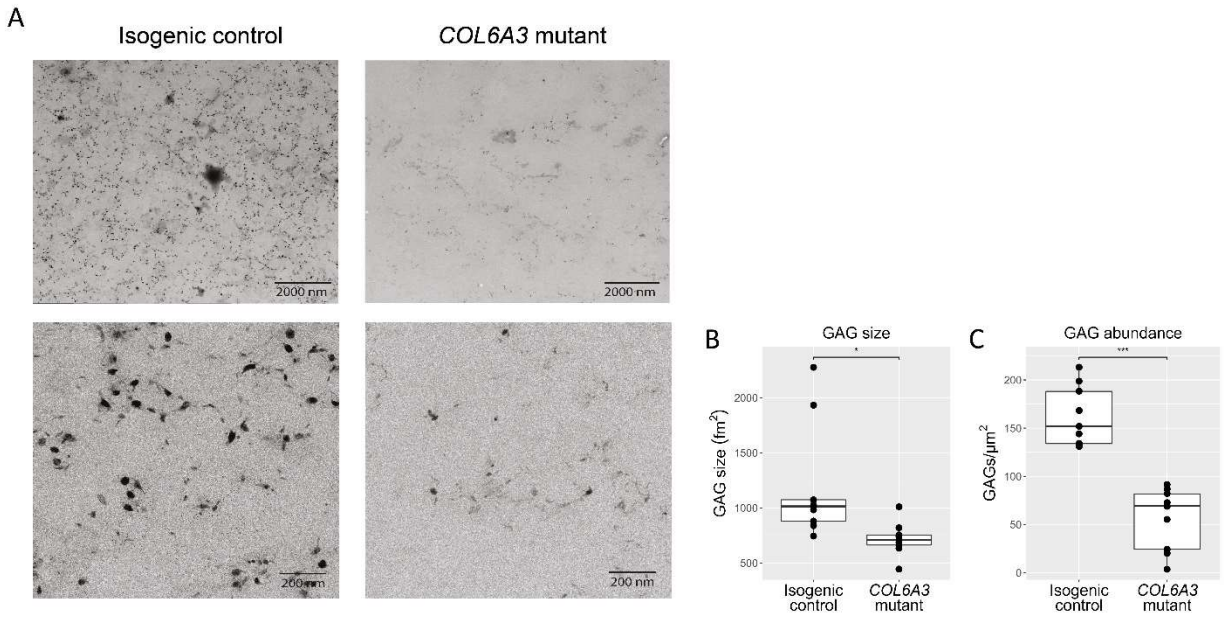

539

540 **Figure 2. The COLVI mutation reduces sGAG aggregate size. (A)** TEM image of isogenic
541 control (left) and a *COL6A3*-mutant (right) neo-cartilage organoid. **(B)** Using a deep-learning
542 algorithm, the sGAG aggregate size was measured, showed a reduction in the *COL6A3*-mutant
543 neo-cartilage organoids (beta=-479.7, P=1.93X10^{-2}). **(C)** GAG amount was decreased in the
544 *COL6A3*-mutant neo-cartilage organoids (beta=-106.14 ± 14.95, P=2.52X10^{-6}). Statistics are
545 reported as beta ± standard error. The box plots represent 25th, 50th, and 75th percentiles, and
546 whiskers extend to 1.5 times the interquartile range. Individual samples are depicted by black dots
547 in each graph. P values were attained using a generalized linear model, with GAG size or
548 GAGs/mm^2 as a dependent variable and genotype as an independent variable.

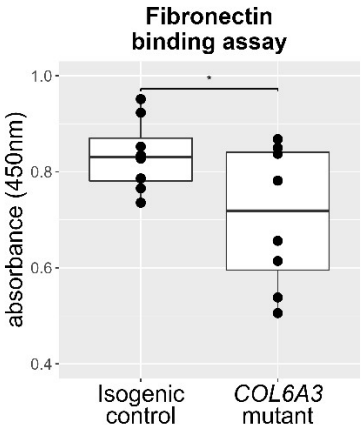

549

550 **Figure 3. The COLVI mutation reduces binding to fibronectin (A)** Solid-phase binding assay
551 with full-length fibronectin-coated wells and wild-type and R1504W mutant COLVI. R1504W
552 showed a reduced binding to fibronectin (beta=-0.13 ± 0.06, P=4.37 x10^{-2}, N=8). This assay did
553 not show binding of COLVI to hyaluronan. Statistics are reported as beta ± standard error. The
554 box plots represent 25th, 50th, and 75th percentiles, and whiskers extend to 1.5 times the
555 interquartile range. Individual samples are depicted by black dots in each graph. P values were
556 attained using a generalized linear model with absorbance at 450nm as dependent variable and
557 genotype as independent variable.

558

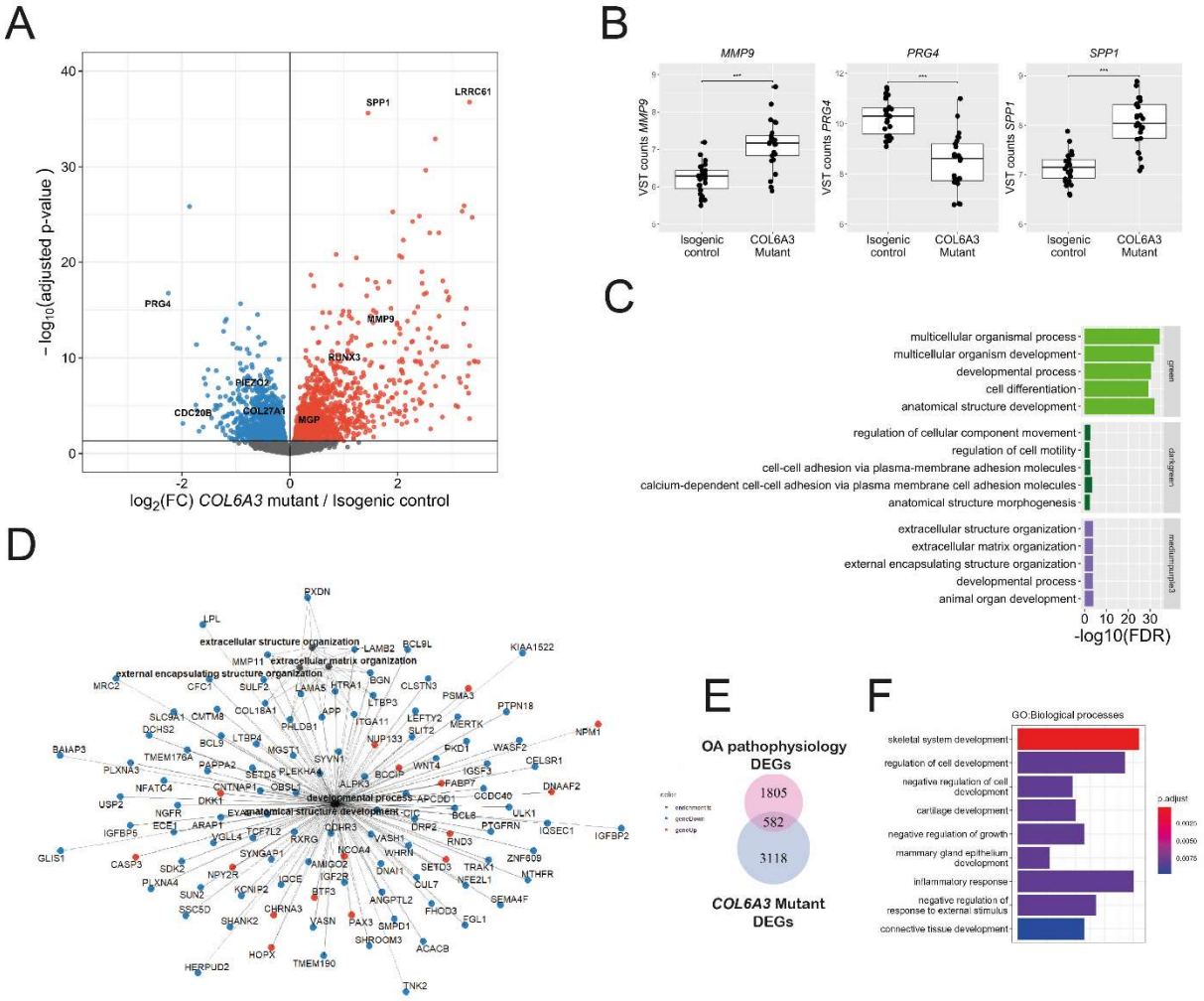

Figure 4. Transcriptomic profile in presence of the *COL6A3* mutation (A) Volcano plot showing the differentially expressed genes (DEGs) in response to the *COL6A3* mutation (N=26). Red dots denote DEGs with an FDR<0.05 that are upregulated, and blue dots represent DEGs that are downregulated, as determined by DESeq2 analysis. **(B)** Notable examples of DEGs between isogenic control and *COL6A3*-mutant neo-cartilage pellets. The box plots represent 25th, 50th, and 75th percentiles, and whiskers extend to 1.5 times the interquartile range. Individual samples are depicted by black dots in each graph. ***FDR<0.001 **(C)** Overrepresentation enrichment analysis (KEGG, REACTOME, GO biological processes) of the top 3 weighted gene co-expression network analysis (WGCNA) co-expression modules where the first principal component is

569 significantly associated with the *COL6A3* mutation. **(D)** Pathway – gene network of the enrichment
570 analysis of the mediumpurple3 cluster. Lines depict the relationship between the genes and the
571 pathways determined by enrichment analysis. Blue dots depict downregulated DEGs with the
572 *COL6A3* mutation, while red dots depict upregulated DEGs with the *COL6A3* mutation. **(E)**
573 Overlap between the *COL6A3* mutation DEGs and differential expression between lesioned and
574 preserved cartilage from a previously published dataset (RAAK study, Ramos et al., 2014). **(F)**
575 Over-representation enrichment analysis of overlapping DEGs between the mutation and lesioned
576 versus preserved cartilage. Count depicts the number of genes that are categorized to each pathway.

577

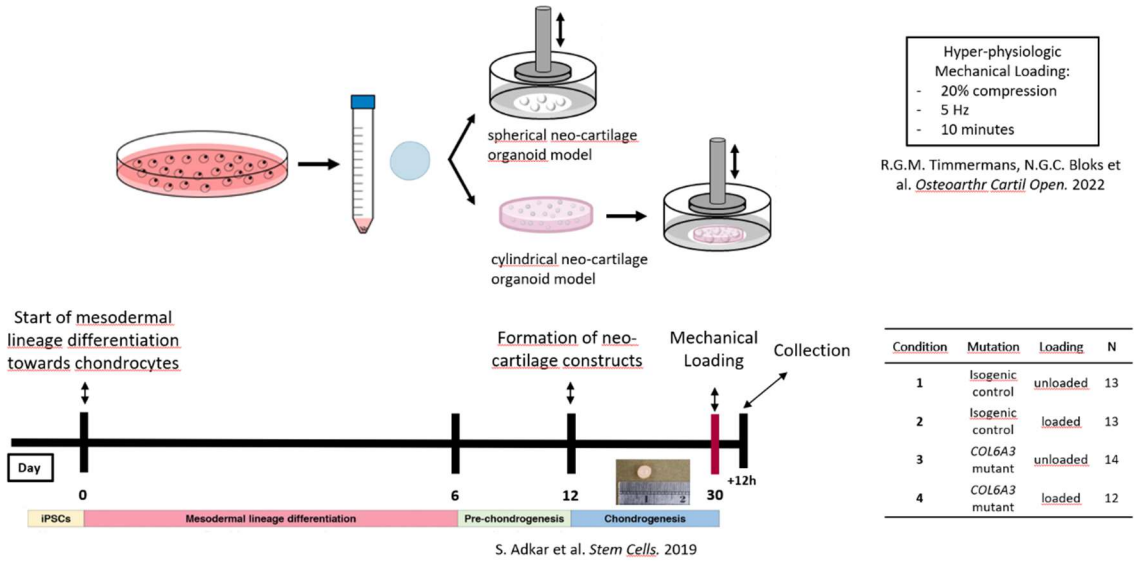

Condition	Mutation	Loading	N
1	Isogenic control	unloaded	13
2	Isogenic control	loaded	13
3	*COL6A3* mutant	unloaded	14
4	*COL6A3* mutant	loaded	12

578

579 **Figure 5. Chondrogenic models to study the effects of aberrant COLVI function in**
580 **interaction with hyper-physiologic mechanical loading conditions.** hiPSCs in which the
581 R1504W mutation was introduced using CRISPR-Cas9 genome editing. These cells were

differentiated using an established differentiation protocol to produce neo-cartilage organoids. Two different organoid models were employed; 1. A spherical pellet model harnessing the original matrix produced by the hiPSCs. 2. A cylindrical organoid model in which the hiPSc-derived chondrocytes were embedded in an agarose construct, ideally suited for testing the effects of mechanical loading conditions. These constructs were both exposed to hyper-physiological loading conditions, after which the organoids were harvested for downstream analysis.

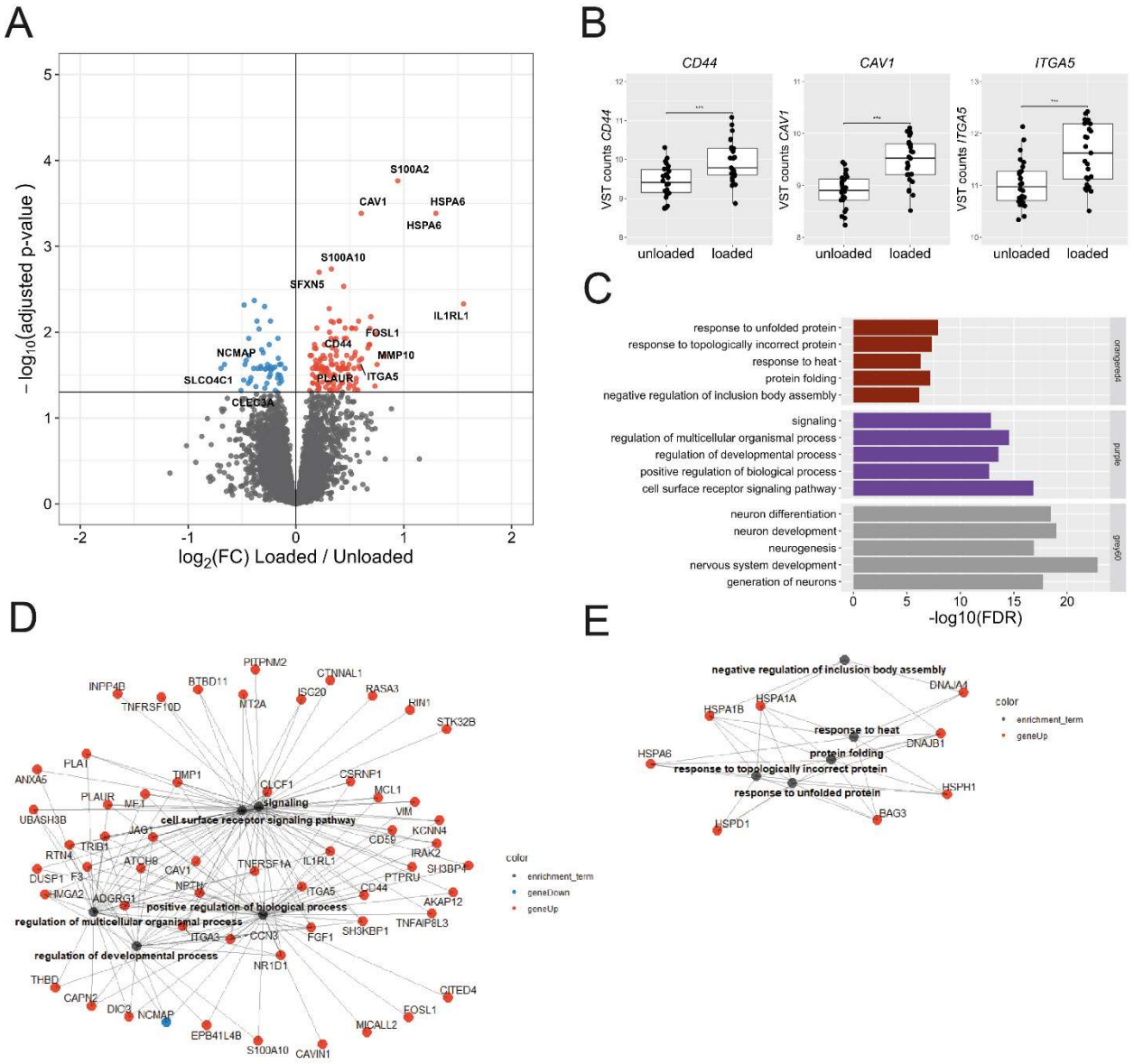

588

589 **Figure 6. Transcriptomic profile in response to hyper-physiologic mechanical loading**
590 **conditions. (A)** Volcano plot of differentially expressed genes (DEGs) in response to hyper-
591 physiologic loading conditions. Red dots denote differentially DEGs with an FDR<0.05 that are
592 upregulated, and blue dots represent DEGs that are downregulated as determined by DESeq2
593 analysis. **(B)** Notable examples of mechano-sensor genes upregulated in response to hyper-
594 physiological mechanical loading conditions. The box plots represent the 25th, 50th, and 75th
595 percentiles, and the whiskers extend to 1.5 times the interquartile range. Individual samples are
596 depicted by black dots in each graph. *FDR<0.05 **(C)** Overrepresentation enrichment analysis
597 (KEGG, REACTOME, GO biological processes) of the top 3 weighted gene co-expression
598 network analysis (WGCNA) co-expression modules of which the first principle component is
599 significantly associated with hyper-physiologic mechanical loading conditions. **(D-E)** Gene-
600 pathway network of the enrichment analysis of the purple **(D)** and the orangered4 **(E)** co-
601 expression network where lines depict the relationship between the genes and the pathways
602 determined by enrichment analysis. Blue dots depict downregulated DEGs in response to hyper-
603 physiologic mechanical loading conditions, red dots depict upregulated DEGs in response to
604 hyper-physiologic mechanical loading conditions.

605

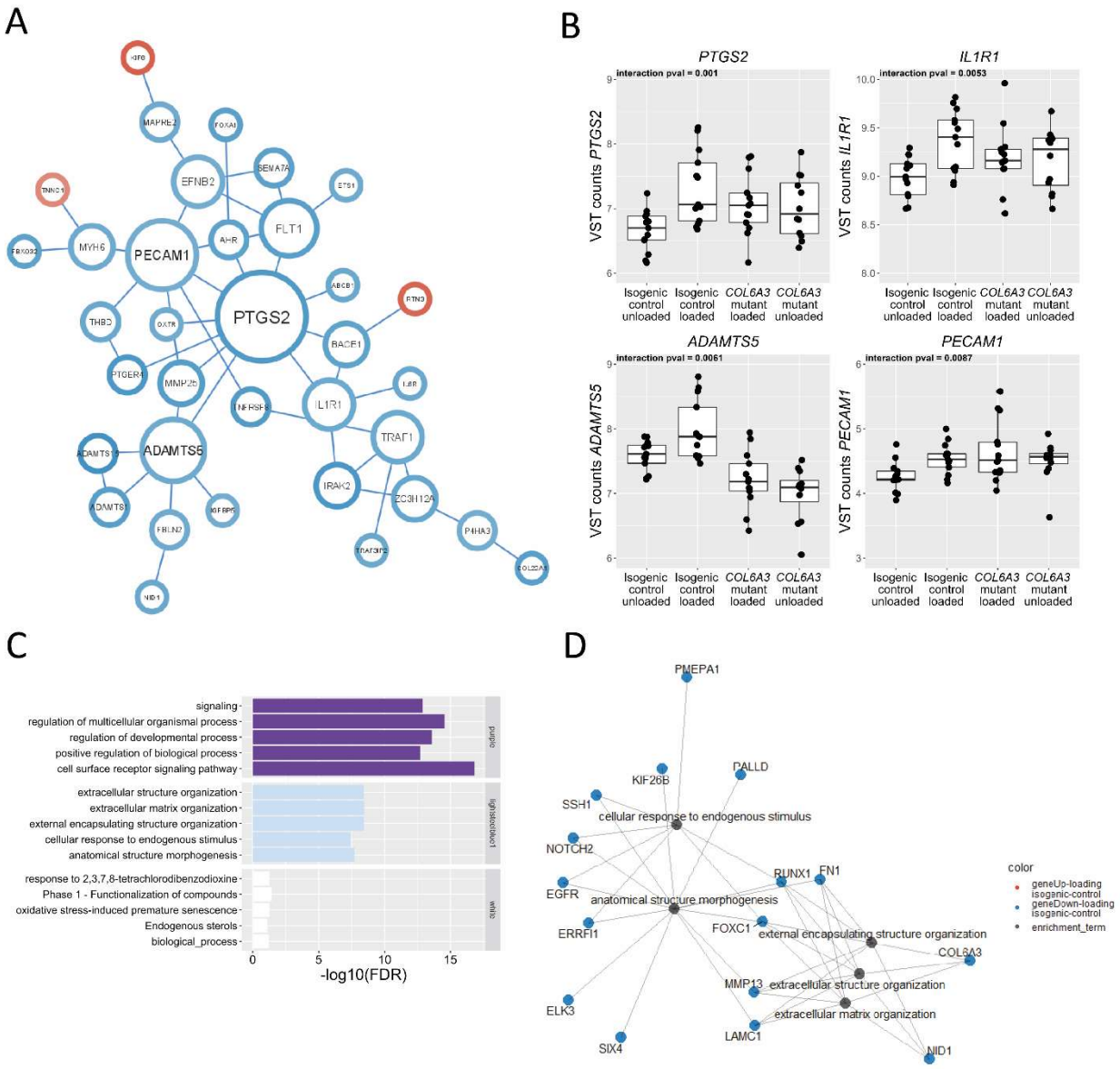

Figure 7. The *COL6A3* mutation affects the biological response to hyper-physiologic loading conditions. **(A)** Protein-protein interaction (PPI) network based on the STRING-DB of genes that show an interaction (P<0.01) between the *COL6A3* mutation and hyper-physiological mechanical loading conditions. Red circles denote an increased response to hyper-physiological mechanical loading due to the *COL6A3* mutation, while blue circles denote a reduced response to mechanical stress due to the *COL6A3* mutation (only showing connected nodes). Relative node size depicts number of connections for each gene within the network **(B)** Examples of central DEGs in the PPI

614 that are related to an inflammatory response. The box plots represent 25th, 50th, and 75th
615 percentiles, and whiskers extend to 1.5 times the interquartile range. Individual samples are
616 depicted by black dots in each graph. **(C)** Gene enrichment analysis of WGCNA hubs significantly
617 related to the interaction between the *COL6A3* mutation and the response to hyper-physiological
618 mechanical loading conditions. **(D)** Pathway – gene network of the enrichment analysis of the
619 purple cluster. Lines depict the relationship between the genes and the pathways determined by
620 enrichment analysis. Blue and red dots depict, respectively, downregulated and upregulated DEGs
621 in response to hyper-physiological loading conditions in the isogenic control neo-cartilage
622 organoids.

623

624 **Table 1. Effect of the *COL6A3* mutation on markers of cartilage metabolism**

	Effect of *COL6A3* genotype		
Gene	**beta**	**SE**	***p*-value**
Catabolic			
MMP13	0.02	0.27	0.94
MMP3	-1.19	0.7	0.09
ADAMTS5	-1.01	0.14	**<0.001**
Anabolic			
COL2A1	-0.47	0.2	**0.02**
ACAN	-0.54	0.21	**0.01**
Hypertrophic			
COL10A1	-0.07	0.16	0.65

625